Carbon 223 (2024) 119015

Contents lists available at ScienceDirect

Carbon

journal homepage: www.elsevier.com/locate/carbon

Engineering phonon transport through cation disorder in dimensionally constricted high entropy MXene

Prince Sharma [a,**], Prashant Singh [b,*], Ganesh Balasubramanian [a]

[a] Department of Mechanical Engineering and Mechanics, Lehigh University, Bethlehem, PA, 18015, USA
[b] Ames National Laboratory, U.S. Department of Energy, Iowa State University, Ames, IA, 50011, USA

ARTICLE INFO

Keywords:
MXene
High entropy materials
Cationic disorder
2D materials
Thermal conductivity

ABSTRACT

Designing materials with low thermal conductivity is a crucial objective for applications in thermal insulation and thermoelectrics. Traditional methods such as doping, mechanical strain and introducing defects in perfect crystals have been widely explored to impede the flow of heat. This work introduces dimensional constriction and cationic disorder as novel avenues to manipulate lattice thermal conductivity (LTC). High entropy materials characterized by random distribution of multiple elements, creates a suitable environment for thermal insulation due to its configurational disorder and local lattice distortions. On the other hand, MXenes, derived from MAX-phase, have garnered considerable attention due to their unique structural attributes, leading to potential applications in catalysis and energy storage. Ti_2AlC MAX-phase is examined to understand the impact of dimensional constriction on phonon transport of Ti_2C with cationic disorder, i.e., $(Ti_{0.25}Nb_{0.25}Cr_{0.25}Ta_{0.25})_2C$. The exponential reduction in LTC of HE-MXene is attributed to disorder scattering that significantly limits phonon mean free path (MFP) and relaxation time. The spread of mode-resolved LTC with MFP highlights the influence of disorder on phonon scattering. This work provides a systematic approach to engineer LTC through dimensional constriction and cationic disorder, laying the foundation for tailored materials with desired thermal properties.

1. Introduction

The incorporation of the concept of high configurational entropy in disordered solids has brought about a revolutionary shift in the realm of alloying and materials design. High entropy materials have been found to possess exceptional properties, for instance, enhanced mechanical strength, improved radiation resistance, and superior thermal stability, making them promising candidates for a wide range of applications in aerospace, energy storage, and structural materials design [1–5]. The configurational disorder or high entropy of mixing, surprises with a latent mass disorder, charge transfer and hence possible electron-phonon coupling. These disorders play a pivotal role in scattering, thereby contributing to the manifestation of low thermal conductivity [6–8].

MAX phases, in the recent past, have also garnered considerable attention, driven by their unique structural properties and promising applications [9–17]. MAX phases, characterized by the general formula $M_{n+1}AlX_n$, where M is an early transition metal, A is an element from groups IIIA and IVA in the periodic table and X is carbon or nitrogen, exhibit a fascinating combination of metallic and ceramic features. On the other hand, MXenes, dimensionally constricted form of MAX phases derived through selective etching, present two-dimensional (2D) structures with versatile properties, making them promising candidates for applications ranging from energy storage to catalysis [11–13,17].

The understanding of the thermal transport of MAX phases and MXenes is crucial for optimizing their performance. Studies have established that MAX phases possess excellent thermal transport properties, primarily attributed to their three-dimensional structures and strong interatomic bonds [18–21]. In previous studies on semiconductor alloys namely SiGe, AlGaAsSb, and InGaAsP, it was found that lowest thermal conductivity was obtained at equiatomic compositions or at the center of composition property diagrams [22–25]. These findings lay an important foundation for understanding of configurational disorder and its effects on thermal conductivity.

* Corresponding author. Ames National Laboratory, 336 Wilhelm Hall, Ames, IA, 50011, USA.
** Corresponding author. 327 Packard Lab, Bethlehem, PA, 18015, USA.
E-mail addresses: prs221@lehigh.edu (P. Sharma), psingh84@ameslab.gov (P. Singh).

https://doi.org/10.1016/j.carbon.2024.119015
Received 4 January 2024; Received in revised form 1 March 2024; Accepted 3 March 2024
Available online 4 March 2024

2. Method

We employ the projector augmented wave (PAW) method within VASP code, for all first principal computations [26,27]. To optimize the unit cell and atomic positions, we make use of the PBE functional [28]. Additionally, we set a high energy cutoff of 550 eV for planewaves expansion. A smearing width of 0.01 eV with the Monkhorst-Pack method is utilized to create a K-point mesh for Brillouin zone integration, aiming for a precision level of 0.03 [29]. An electronic convergence criterion 10^{-6} eV was set between two self-consistent loop and an ionic convergence criterion of 10^{-4} eV was set to obtain a structure without residual forces for phonon calculations. Phonopy and Phono3py code were employed to create displacement based on frozen phonon model to calculate thermal properties [30–34]. A 2 × 2 × 2 supercell with 64 atoms is used for Ti_2AlC max phase and for Ti_2C MXene monolayer, a 4 × 4 × 1 supercell containing 48 atom is used for all phonon calculations. A randomly disordered unitcell of $(Ti_{0.25}Nb_{0.25}Cr_{0.25}Ta_{0.25})_2C$ HE-MXene monolayer was created using ATAT enabled mcsqs [35]. More details about thermal conductivity convergence test with respect to increasing nearest-neighbor (4th nearest neighbor cutoff) interactions for HE-MXene monolayer (48 atoms supercell of dimensions 2 × 2 × 1) is employed with cutoff (see Supplementary Fig. 5).

3. Results

The effect of dimensional, atomic, and configurational complexities on lattice thermal conductivity: Fig. 1(a–c) are schematic representation of a simple cubic lattice with 1st nearest neighbor phonons followed by loss of phonons due to dimensional constriction and finally fluctuations of mass and force constants due to cationic disorder. This work extends our understanding to the realm of high-entropy MXenes (HE-MXene), where the introduction of multiple cationic species (Ti, Nb, Cr, and Ta) induces a distorted structure. This local lattice distortion, a key feature in HE-MXene, playing a crucial role in understanding variations in interatomic force constants. The intricate interplay between structural distortions and cationic disorder, in Ti-based MAX phases, Ti_2AlC, Ti_2C, and a high-entropy variant $(Ti_{0.25}Nb_{0.25}Cr_{0.25}Ta_{0.25})_2C$ is correlated with thermal conductivity. Thus, the creation of a complex electronic and physical environment in HE-MXene contributes to the observed anisotropy in thermal transport and low thermal conductivity. We employ Phono3py code interfaced with first-principles density-functional theory as implemented within Vienna Ab-initio Simulation Package (VASP) [26,31] to calculate thermal transport of both bulk and dimensionally reduced MAX phases.

Fig. 1(d–f) shows relaxed Ti_2AlC, Ti_2C and $(Ti_{0.25}Nb_{0.25}Cr_{0.25}Ta_{0.25})_2C$ structures, respectively. The Ti_2AlC is in hexagonal phase with $P6_3/mmc$ space group symmetry where leaching out Al and increase in interlayer separation between two Ti_2C layers reduces the symmetry operations. While $(Ti_{0.25}Nb_{0.25}Cr_{0.25}Ta_{0.25})_2C$ is devoid of any symmetry due to chemical disorder on inversion symmetry points. Clearly, the relaxed structures of MAX phase and MXene are arranged devoid of local atomic displacements while the HE-MXene assumes a distorted structure by incorporation of multiple cationic species in the well-arranged MXene lattice. This distortion further proves to be an important factor

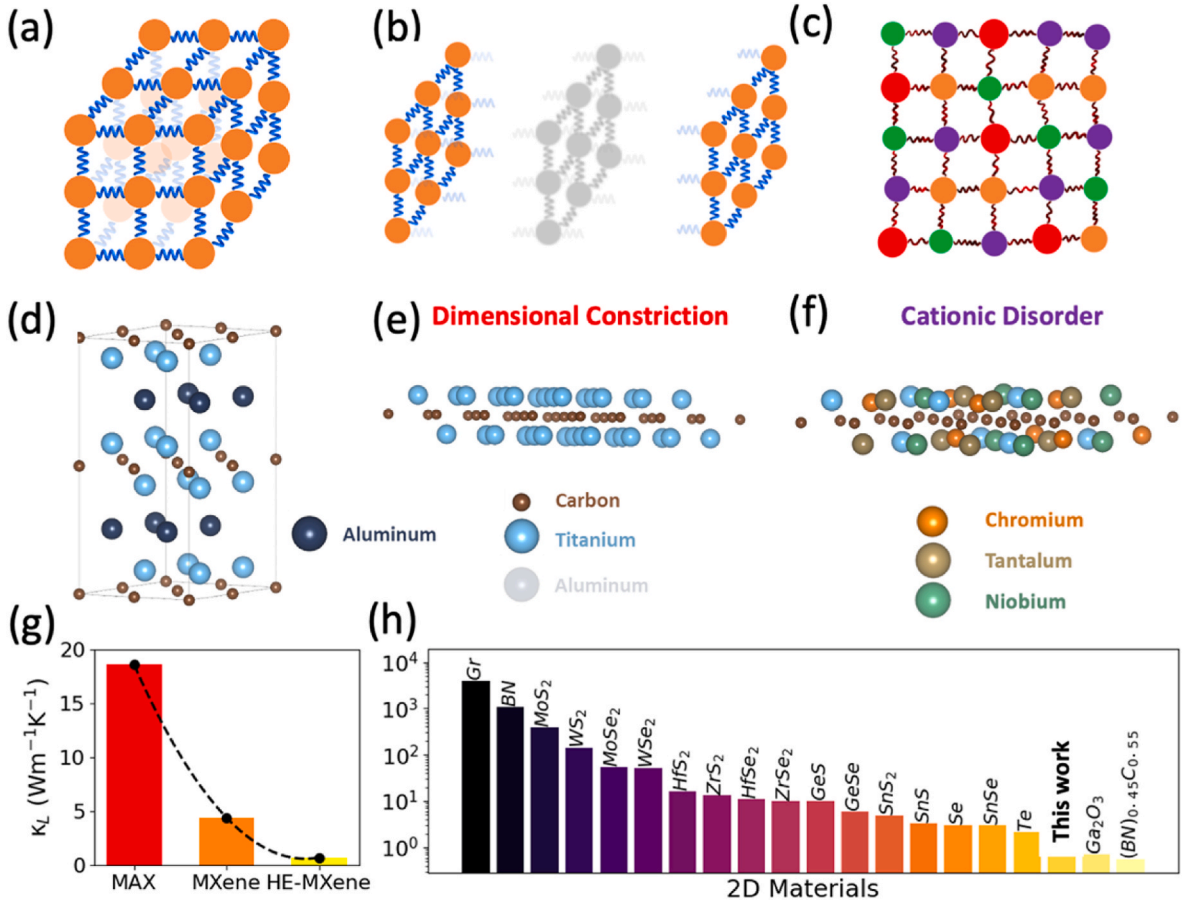

Fig. 1. (a) a visual representation of first nearest neighbor phonons in a simple cubic system; (b) a schematic illustrating zero force constants for a monolayers or surfaces with sufficiently large interlayer distances; (c) a 2D projected schematic of high entropy configuration (atomic species are represented by different colors), creating a non-uniform phononic environment due to variations in force constants. Crystal structures of (d) Ti_2AlC MAX phase, (e) a dimensionally constricted Ti_2C monolayer, and (f) monolayer of $(Ti_{0.25}Nb_{0.25}Cr_{0.25}Ta_{0.25})_2C$ HE-MXene. The bar graphs highlighting (g) the impact of dimensional constriction and cationic disorder on LTC at RT, and (h) comparison with 2D literature data [38–46].

for variations in interatomic force constants in the frozen phonon model employed for calculation of thermal conductivity, similar behavior has been noted by Refs. [36,37].

The reduction of thermal conductivity at room temperature for the 2D monolayers due to dimensional constriction and cationic disorder is shown in Fig. 1(g). LTC near RT for Ti_2AlC MAX is found to be 18.589 $Wm^{-1}K^{-1}$ which agrees with literature values of 12–26 $Wm^{-1}K^{-1}$ [47,48] while LTC for monolayer Ti_2C MXene 4.14 $Wm^{-1}K^{-1}$. On the other hand, the LTC of $(Ti_{0.25}Nb_{0.25}Cr_{0.25}Ta_{0.25})_2C$ HE-MXene is 0.696 $Wm^{-1}K^{-1}$, which shows significant reduction compared to both bulk MAX and monolayer MXene. Fig. 1(h) displays a comparative analysis of thermal conductivity values from literature, including those for HE-MXene as reported in this study. As per Slack's observations, achieving high thermal conductivity in non-metallic systems requires a combination of factors: low atomic mass, strong interatomic bonding, a simple crystal structure (i.e., fewer atoms per unit cell), and low anharmonicity [49]. Examining materials like graphene (Gr), BN, MoS_2, and WS_2, we observe that Gr boasts the highest thermal conductivity, attributed to its simple 2D hexagonal layer comprising strongly sp^2-bonded low atomic mass carbons. Conversely, in materials like BN, where nitrogen introduces higher atomic mass (compared to carbon), thermal conductivity decreases. This trend is similarly evident in MoS_2 and WS_2. In the case of MXene and HE-MXene, the crystal structure's simplicity is compromised, and bonding weakens due to charge distortions. Furthermore, the presence of a free surface enhances anharmonicity, and the incorporation of Cr, Ta, and Nb increases the average atomic mass of cations. Collectively, these factors contribute to the diminished thermal conductivity observed in HE-MXene.

Phonon dispersion of Ti_2AlC MAX, Ti_2C MXene, and $(Ti_{0.25}Nb_{0.25}Cr_{0.25}Ta_{0.25})_2C$ HE-MXene: Fig. 2(a–c) shows phonon spectral functions for the three material classes in Fig. 1(d–f). The highest assumed frequency for MAX phase is around 20.4 THz while we observe a reduction to 19.53 THz for MXene due to absence of Aluminum and dimensional constriction via introduction of large van der Waals gap. In case of HE-MXene due to combinatorial effect of local lattice distortions and multiple cations namely, Ti, Nb, Cr and Ta, creates fluctuations in force constants. There is systematic decrement in the acoustic band frequencies from MAX phase to HE-MXene. Also, the spectral width of optical bands in MXene is minimal due to uniform chemical environment around carbon atoms while the spectral widths increase due to force constant and mass fluctuations that arises when bonds are distorted due to doping of atomic species on Ti sites. Consequently, the dispersion of optical bands increases in HE-MXene as seen in Fig. 2(c). This is also inferred from phonon density of states (Supplementary Fig. 1) that the contribution to optical band from all C atoms is nearly equal while in case of HE-MXene, there are four peaks with each having been dominated by a particular carbon atom. After careful examination of normal mode-frequency band, the frequencies systematically decrease from MAX phase to MXene. This is in accordance with Rayleigh's theorem, as creation of free surface reduces force constant to zero and hence leading to increased amplitude of vibration, finally resulting in drop of one of optical frequency [50,51]. However, creation of high entropy surfaces in HE-MXene overcomes this drop due to an uneven surface and distortion. The straight optical bands in MXene are due to the high mass ratio (≈4) of Ti and C and the same behaviors can be seen in other compounds as well [52].

***Temperature dependent lattice thermal conductivity and band-specific MFP at RT*:** Fig. 3(a–c) shows variation in thermal conductivity tensor with temperature for Ti_2AlC MAX, Ti2C and HE-MXene. MAX phase shows superior phonon transport in in-plane direction (x,y) compared to out-of-plane (z) direction. The reduced LTC in orthogonal direction for the MAX is primarily due to week Al and Ti_2C bonding (inferred from Supplementary Fig. 2), hence a weaker force constant enabling lower thermal transport. The Al pairs show least trace value of force constant matrix (see Supplementary Fig. 3) which proves that Al atoms are loosely bonded. Ti_2C MXene shows lower LTC compared to MAX phase because of significant reduction of vibrational modes and enhanced surface scattering effects. The LTC is further reduced due to enhanced scattering enabled by complex electronic and physical environment due to cationic disorder, i.e., a disorder comprising of mass disorder with electron-phonon coupling.

We notice an anisotropy in thermal transport in HE-MXene, Fig. 3 (a–c), it originates from fluctuation in force constants as shown in Supplementary Fig. 3(c). Most of scatter points in force constants coincide in case of Ti_2C MXene (Supplementary Fig. 3b) while there are slight deviations in, HE-MXene. Additionally, the lattice distortion also modifies the charge distortion and further increases anisotropy (see Supplementary Figs. 2(e–f)), the charge distribution is homogeneous in the directions of lattice vectors while it loses homogeneity in case of, HE-MXene, giving rise to anisotropic phonon transportation [53,54]. The mass disorder is different in all direction due to random distribution of elements on atomic lattices. The decrease in the LTC observed in HE-MXene can be attributed to a significant constraint arising from substantial heat capacity contributions occurring within a relatively confined frequency range, as illustrated in Supplementary Fig. 4. This phenomenon is closely linked to the degeneracy observed in the band structures [55–58]. This relationship implies large anharmonicity and an augmented occurrence of Umklapp Scattering [59,60].

Fig. 3(d–f) shows the spread of mode resolved LTC with MFP. In MAX phase, the 3D structure assumes the largest mean free path, while the dimensional restrictions imposed on MXene depreciate the MFP. This effect is further amplified for HE-MXene. Notably, in the context of MAX phases, mid-range frequencies, primarily associated with non-planar modes of vibration, play a significant role in contributing the most to LTC.

Conversely, when examining MXene, confinement-induced reduction of non-planar phonon modes diminishes the impact of mid-range frequencies. Despite this reduction, the lower number of phonon modes facilitates the efficient transport of thermal energy, as evidenced by the notably high κ_L in Fig. 3(e). This contrasts with MAX phase, where

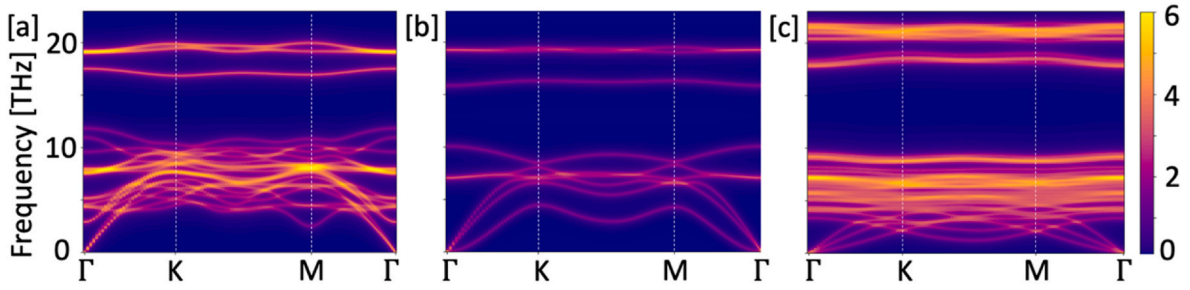

Fig. 2. (a) Ti_2AlC MAX displays pronounced dispersion in areas with overlapping bands that reflects ability to accommodate numerous phonon modes, (b) Ti_2C MXene exhibits minimal dispersion which is attributed to the uniform arrangement of titanium (Ti) and carbon (C) atoms in 2D lattice, and (c) $(Ti_{0.25}Nb_{0.25}Cr_{0.25}Ta_{0.25})_2C$ HE-MXene exhibits a substantial dispersion in the phonon band structure. This dispersion is a consequence of fluctuations in masses and force constants, stemming from the presence of multiple cations and local lattice distortions within the HE-MXene.

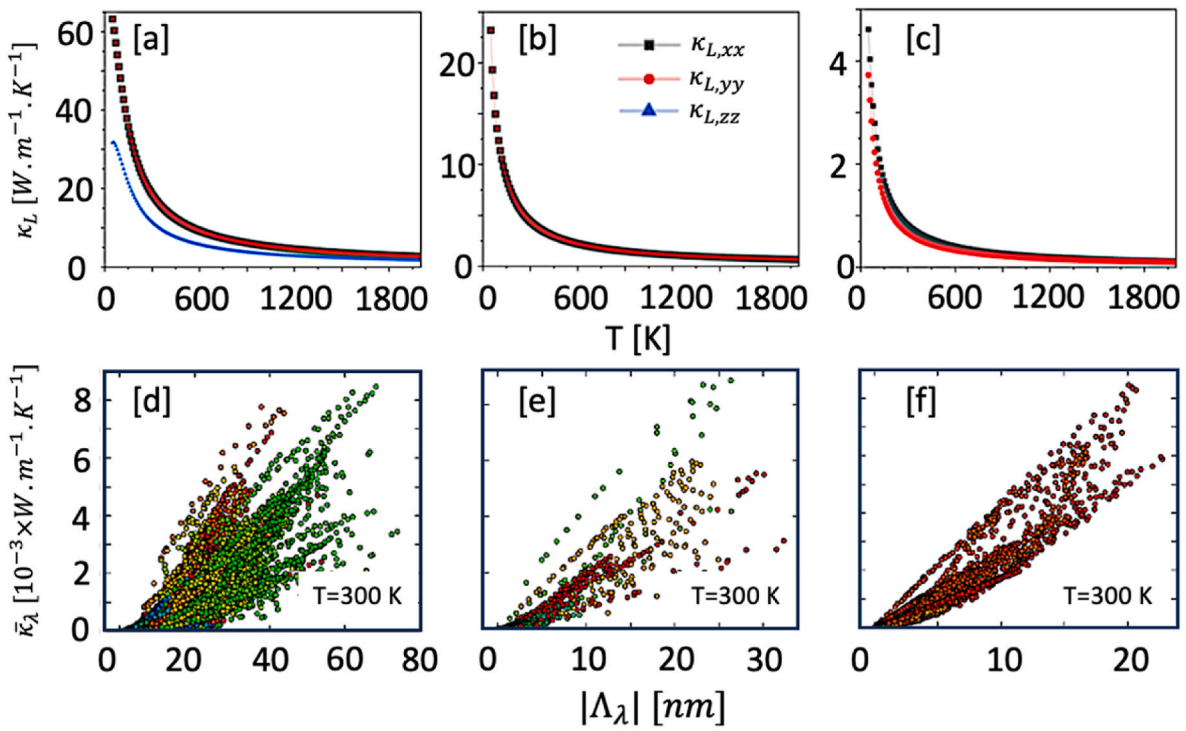

Fig. 3. (a) Bulk Ti_2AlC MAX showing higher in in-plane (xx, yy) κ_L while out-of-plane component takes slightly lower LTC. (b) A significantly reduced κ_L for Ti_2C MXene is attributed to dimensional confinement compared to MAX phase. (c) Disordered HE-MXene exhibits the lowest thermal conductivity, characterized by anisotropy stemming from the broken inversion symmetry of 2D lattice. The alloying effect leads to increased mass and force constant fluctuations, enabling disorder broadening of dispersion (Fig. 2). (d–f) The significant impact of MFP for different phonons on the thermal conductivity (κ_L) of various materials. The contribution to κ_L depends on the magnitude of MFP, MAX-phase due to highest MFP for most phonons possess largest κ_L while HE-MXene due to lowest MFP possess low thermal conductivity.

the largest contribution to the LTC comes from mid-range frequency bands, particularly out-of-plane vibrational modes represented by green dots. When dimensional constriction reduces out-of-plane vibrational modes, the remaining other modes can now carry a larger amount of vibrational energy for mid-range frequencies, as illustrated in Fig. 3(e).

Quantitatively, there is a substantial reduction in MFP from

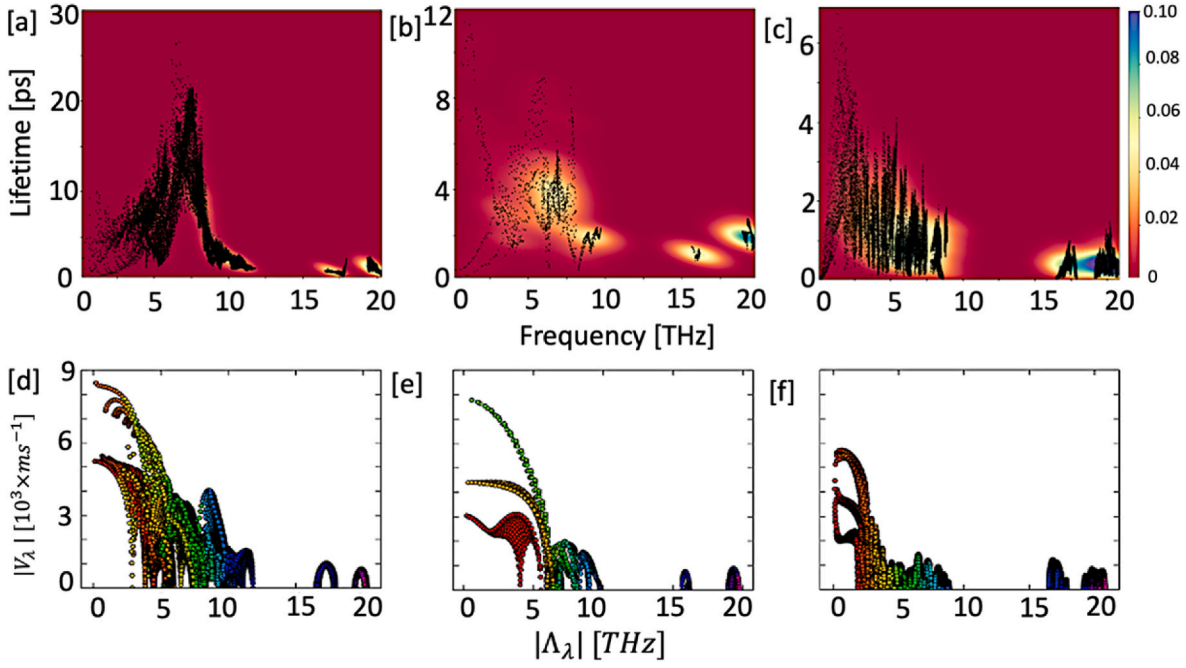

Fig. 4. (a–c) Phonon lifetimes, measured in picoseconds (ps), are significantly reduced in going from bulk Ti_2AlC MAX to HE-MXene. The peak in phonon lifetime ramps down from 25 ps for Ti_2AlC MAX to 2 ps for HE-MXene, respectively. (d–f) Similar to phonon lifetime, MAX phase displays substantially large group velocities at lower frequencies, primarily attributed to modes associated with metallic bonded Al compared toTi_2C and HE MXenes. The significant drop in group velocities of HE-MXene was attributed to non-uniform phonon frequencies compared to MAX, a consequence of atomic heterogeneities.

approximately 78 nm MAX phase) to around 7.8 nm (HE-MXene) at 300K. This reduction can be attributed to variations in mass and phonon frequency. It is evident that in the MAX phase, a significant amount of thermal energy is transferred through moderate-frequency bands, while in HE-MXene, higher-frequency bands assume a more prominent role in facilitating the transport of energy. Nevertheless, due to lower number of modes, the cumulative effect on LTC is not large. In case of HE-MXene, the low frequency modes contribute largest because of the fact that off-layer modes and maximum force constants are not homogenous anymore due to complex electronic (cations) and physical (masses and atomic radii) environment. This shows a systematic way to engineer LTC by manipulating interatomic force constants and vibrational mode through dimensional constriction and cationic disorder.

Phonon lifetime and group velocity variations with respect to phonon frequencies: Fig. 4(a–c) shows density plot of phonon relaxation lifetimes with respect to phonon frequencies. MAX phase shows largest relaxation times which is reduced by ~60% for MXene and further reduced to 10% for HE-MXene. The increased number of modes in HE-MXene due to breaking of symmetry increases the number of phonon modes in Fig. 4(c) nevertheless, it has significantly reduced relaxation time. The order-of-magnitude drop in phonon lifetime (Fig. 4(c)) of dimensionally reduced HE-MXene is attributed to rugged averaging effect, a key attribute of high-entropy alloying, that leads to increased mass and force constant fluctuations.

Notably, a structure with lower symmetry is prone to strain disorder as compared to the one with higher symmetry (Fig. 1(c) and .(f)). This is also related to disorder scattering that lowers the MFP of phonons as shown in Fig. 3. In highly disordered systems, the scattering is proportion to the fourth power of vibrational frequency hence all the energy is transported by low frequency phonons [61,62].

The disorder alloying of Ti site in dimensionally reduced MAX with group V (Ta, Nb) and group VI (Cr) elements pumps in excess valence electrons into the 2D lattice. The interactions between excess electrons and phonons at finite temperature leads to reduced MFP in HE-MXene. The significant fall in LTC is due to additional loss from strain scattering caused by local lattice distortion by size-mismatch elements in HE-MXene. Finally, the trend in relaxation time can be related to inhomogeneity of bond strength, force constants fluctuations, mass disorder and lattice distortions. Furthermore, we also note a reduction of group velocities for band specific phonon modes as shown in Fig. 4(d–e). Mid-range frequency bands (red, orange and yellow) show decrement in group velocities as one moves from 3D MAX phase structure to 2D MXene and further to cation-disordered HE-MXene. A reduction in frequencies of acoustic bands is prominently visible in Fig. 4(d–f) and Fig. 2 (a–c).

4. Discussion and summary

This study investigates the effects of configurational [63] and dimensional modifications on LTC. We show that via dimensional constriction, LTC of a material can be significantly reduced. The further reduction in thermal conductivity at room temperature for HE-MXene 2D monolayers, attributed to cationic disorder, is noteworthy. Here, the merger of concepts from phonon engineering and high entropy alloying to obtain materials with ultra-low LTC is successfully demonstrated. Dimensional constriction not only limits the number of vibrational modes but also increases boundary scattering by the virtue of free surface creation. Ti_2C MXene exhibits lower LTC due to reduced vibrational modes and enhanced surface scattering effects. Further to modulate the magnitude of LTC in dimensionally constricted MXene, cationic disorder is created on Ti sites. Multiple cations with different mass and atomic numbers induce mass disorder scattering as well as enhanced electron-phonon coupling with local lattice distortion. These disorders and distortion, vividly captured in the phonon spectral functions becomes imperative for understanding the variations in thermal conductivity. The mass disorder scattering along with charge transfer reduces the LTC nearly by six times in HE-MXene compared to bulk Ti_2AlC MAX and Ti_2C MXene. These disorders not only reduce LTC but also makes the system anisotropic, which is widely known property of such material class [40,53,54,64]. Furthermore, the average LTC for HE-MXene was also calculated on four distinct random structures. The DFT calculated LTC values along with their means, errors, and variations across temperature ranges are provided in Supplemental Fig. 6. It is noteworthy that all four structures are configurationally different and exhibit a complete absence of translational and rotational symmetries, yet remarkably, they yield comparable thermal conductivity values. Furthermore, we want to emphasize on an interesting observation that the error margins at higher temperatures are even smaller or negligible. Notably, the type of disorders, particularly those arising from cationic heterogeneities, present an intriguing avenue for leveraging the concept of compositionally graded materials. By strategically introducing controlled variations in composition, one can manipulate and alter structural disorder to craft materials exhibiting tailored thermal conductivities along specific directions.

The spread of mode resolved LTC with MFP highlights the impact of disorder scattering on thermal transport. MAX phase exhibits the largest MFP due to their ordered crystalline structure, while the dimensional restrictions imposed on MXene and further with configurational disorder in HE-MXene contribute to the reduction in MFP. The density plot of phonon relaxation time with phonon frequencies demonstrates a significant reduction from MAX phase to MXene and lowest for HE-MXene. The increased number of modes in HE-MXene does not compensate for the reduction in relaxation time, highlighting the effect of cationic disorder on phonon relaxation and emphasizes the influence of structural complexity. The reduction in group velocities for band-specific phonon modes corroborates the trend observed in the relaxation times, indicating a fundamental connection between structural disorder and thermal properties.

Finally, our findings underscore importance of structural distortions and cationic disorder in influencing thermal transport properties. The systematic way to engineer LTC, by manipulating interatomic force constants, mass fluctuations and vibrational modes through dimensional constriction and cationic disorder, opens avenues for tailored ultra-low LTC materials. This study provides a foundation for understanding how specific structural modifications can be employed to achieve desired thermal properties in advanced engineering materials.

Data availability

The authors will make available, upon request, the data used in the applications described in this work. It is understood that the data provided will not be employed for commercial use.

Code availability

The authors will make available, upon request, the code used in the applications described in this work. It is understood that the code will not be employed for commercial use.

CRediT authorship contribution statement

Prince Sharma: Writing – original draft, Visualization, Validation, Software, Methodology, Investigation, Formal analysis, Data curation, Conceptualization. **Prashant Singh:** Writing – review & editing, Supervision, Investigation, Funding acquisition, Formal analysis, Conceptualization. **Ganesh Balasubramanian:** Writing – review & editing, Supervision, Resources, Project administration, Funding acquisition, Conceptualization.

Declaration of competing interest

The authors declare that they have no known competing financial

interests or personal relationships that could have appeared to influence the work reported in this paper.

Acknowledgements

The work at Lehigh University was supported in part by the National Science Foundation (NSF) award #CMMI-1944040. Prashant Singh acknowledges funding support in part (related to the effect of distortion on electronic and structural properties of refractory based alloys) to the Laboratory Directed Research and Development (LDRD) program at Ames National Laboratory. The work at Ames National Laboratory was supported by DOE Office of Science, Basic Energy Sciences, Materials Science and Engineering Division. Ames Laboratory is operated by Iowa State University for the U.S. DOE, Office of Science, Office of Basic Energy Sciences under contract DE-AC02-07CH11358.

Appendix A. Supplementary data

Supplementary data to this article can be found online at https://doi.org/10.1016/j.carbon.2024.119015.

References

[1] B. Jiang, Y. Yu, J. Cui, X. Liu, L. Xie, J. Liao, Q. Zhang, Y. Huang, S. Ning, B. Jia, B. Zhu, S. Bai, L. Chen, S.J. Pennycook, J. He, High-entropy-stabilized chalcogenides with high thermoelectric performance, Science 371 (2021) 830–834, https://doi.org/10.1126/science.abe1292.

[2] Z. Fu, L. Jiang, J.L. Wardini, B.E. MacDonald, H. Wen, W. Xiong, D. Zhang, Y. Zhou, T.J. Rupert, W. Chen, E.J. Lavernia, A high-entropy alloy with hierarchical nanoprecipitates and ultrahigh strength, Sci. Adv. 4 (2018) eaat8712, https://doi.org/10.1126/sciadv.aat8712.

[3] D. Shin, S. Chae, S. Park, B. Seo, W. Choi, Rational engineering of high-entropy oxides for Li-ion battery anodes with finely tuned combustion syntheses, NPG Asia Mater. 15 (2023) 54, https://doi.org/10.1038/s41427-023-00502-y.

[4] A. Sarkar, L. Velasco, D. Wang, Q. Wang, G. Talasila, L. de Biasi, C. Kübel, T. Brezesinski, S.S. Bhattacharya, H. Hahn, B. Breitung, High entropy oxides for reversible energy storage, Nat. Commun. 9 (2018) 3400, https://doi.org/10.1038/s41467-018-05774-5.

[5] O. El-Atwani, N. Li, M. Li, A. Devaraj, J.K.S. Baldwin, M.M. Schneider, D. Sobieraj, J.S. Wróbel, D. Nguyen-Manh, S.A. Maloy, E. Martinez, Outstanding radiation resistance of tungsten-based high-entropy alloys, Sci. Adv. 5 (2019) eaav2002, https://doi.org/10.1126/sciadv.aav2002.

[6] X. Qian, J. Zhou, G. Chen, Phonon-engineered extreme thermal conductivity materials, Nat. Mater. 20 (2021) 1188–1202, https://doi.org/10.1038/s41563-021-00918-3.

[7] D. Song, T. Song, U. Paik, G. Lyu, Y.-G. Jung, H.-B. Jeon, Y.-S. Oh, Glass-like thermal conductivity in mass-disordered high-entropy $(Y,Yb)_2(Ti, Zr, Hf)_2O_7$ for thermal barrier material, Mater. Des. 210 (2021) 110059, https://doi.org/10.1016/j.matdes.2021.110059.

[8] J. Garg, N. Bonini, B. Kozinsky, N. Marzari, Role of disorder and anharmonicity in the thermal conductivity of silicon-germanium alloys: a first-principles study, Phys. Rev. Lett. 106 (2011) 045901, https://doi.org/10.1103/PhysRevLett.106.045901.

[9] K. Ghosh, P.K. Giri, Experimental and theoretical study on the role of 2D $Ti_3C_2T_x$ MXenes on superior charge transport and ultra-broadband photodetection in MXene/Bi_2S_3 nanorod composite through local Schottky junctions, Carbon 216 (2024) 118515, https://doi.org/10.1016/j.carbon.2023.118515.

[10] Q. Li, M. Xu, C. Jiang, S. Song, T. Li, M. Sun, W. Chen, H. Peng, Highly sensitive graphene-based ammonia sensor enhanced by electrophoretic deposition of MXene, Carbon 202 (2023) 561–570, https://doi.org/10.1016/j.carbon.2022.11.033.

[11] J. Zhang, Y. Zhao, X. Guo, C. Chen, C.-L. Dong, R.-S. Liu, C.-P. Han, Y. Li, Y. Gogotsi, G. Wang, Single platinum atoms immobilized on an MXene as an efficient catalyst for the hydrogen evolution reaction, Nat. Catal. 1 (2018) 985–992, https://doi.org/10.1038/s41929-018-0195-1.

[12] X. Pan, X. Yang, M. Yu, X. Lu, H. Kang, M.-Q. Yang, Q. Qian, X. Zhao, S. Liang, Z. Bian, 2D MXenes polar catalysts for multi-renewable energy harvesting applications, Nat. Commun. 14 (2023) 4183, https://doi.org/10.1038/s41467-023-39791-w.

[13] A. Bhat, S. Anwer, K.S. Bhat, M.I.H. Mohideen, K. Liao, A. Qurashi, Prospects challenges and stability of 2D MXenes for clean energy conversion and storage applications, NPJ 2D Mater Appl 5 (2021) 61, https://doi.org/10.1038/s41699-021-00239-8.

[14] Y. Lu, X. Zhao, Y. Lin, P. Li, Y. Tao, Z. Wang, J. Ma, H. Xu, Y. Liu, Lightweight MXene/carbon composite foam with hollow skeleton for air-stable, high-temperature-resistant and compressible electromagnetic interference shielding, Carbon 206 (2023) 375–382, https://doi.org/10.1016/j.carbon.2023.02.061.

[15] P. He, Q. Zhou, X.-Y. Zhao, H. Wang, Y. Hu, W. Younas, G.-B. Mao, F. Tao, X.-Y. Qian, F. Wang, Z.-Y. Liu, M.-J. Zheng, Q. Liu, W.-Q. Cao, Z.-L. Hou, J. Yuan, M.-S. Cao, MXene for multifunctional electromagnetic protection, Carbon 213 (2023) 118218, https://doi.org/10.1016/j.carbon.2023.118218.

[16] X. Li, M. Li, X. Li, X. Fan, C. Zhi, Low infrared emissivity and strong stealth of Ti-based MXenes, Research 2022 (2022) 9892628, https://doi.org/10.34133/2022/9892628.

[17] B. Anasori, M.R. Lukatskaya, Y. Gogotsi, 2D metal carbides and nitrides (MXenes) for energy storage, Nat. Rev. Mater. 2 (2017) 16098, https://doi.org/10.1038/natrevmats.2016.98.

[18] G.Ya Khadzhai, R.V. Vovk, T.A. Prichna, E.S. Gevorkyan, M.V. Kislitsa, A. L. Solovjov, Electrical and thermal conductivity of the Ti_3AlC_2 MAX phase at low temperatures, Low Temp. Phys. 44 (2018) 451–452, https://doi.org/10.1063/1.5034158.

[19] R.V. Vovk, G.Ya Khadzhai, T.A. Prikhna, E.S. Gevorkyan, M.V. Kislitsa, A. L. Soloviev, I.L. Goulatis, A. Chroneos, Charge and heat transfer of the Ti_3AlC_2 MAX phase, J. Mater. Sci. Mater. Electron. 29 (2018) 11478–11481, https://doi.org/10.1007/s10854-018-9242-6.

[20] C. Dhakal, S. Aryal, R. Sakidja, W.-Y. Ching, Approximate lattice thermal conductivity of MAX phases at high temperature, J. Eur. Ceram. Soc. 35 (2015) 3203–3212, https://doi.org/10.1016/j.jeurceramsoc.2015.04.013.

[21] L. Yu, L. Xu, L. Lu, Z. Alhalili, X. Zhou, Thermal properties of MXenes and relevant applications, ChemPhysChem. 23 (2022) e202200203, https://doi.org/10.1002/cphc.202200203.

[22] S. Adachi, Lattice thermal resistivity of III–V compound alloys, J. Appl. Phys. 54 (1983) 1844–1848, https://doi.org/10.1063/1.332820.

[23] W. Both, V. Gottschalch, G. Wagner, Thermal resistivity of GaInAsP alloy. Experimental results, Cryst. Res. Technol. 21 (1986) K85–K87, https://doi.org/10.1002/crat.2170210532.

[24] W. Both, A.E. Bochkarev, A.E. Drakin, B.N. Sverdlov, Thermal resistivity of quaternary solid solutions InGaAsSb and GaAlAsSb lattice-matched to GaSb, Cryst. Res. Technol. 24 (1989) K161–K166, https://doi.org/10.1002/crat.2170240921.

[25] A. Skye, P.K. Schelling, Thermal resistivity of Si–Ge alloys by molecular-dynamics simulation, J. Appl. Phys. 103 (2008) 113524, https://doi.org/10.1063/1.2936868.

[26] J. Hafner, Ab-initio simulations of materials using VASP: density-functional theory and beyond, J. Comput. Chem. 29 (2008) 2044–2078, https://doi.org/10.1002/JCC.21057.

[27] G. Kresse, D. Joubert, From ultrasoft pseudopotentials to the projector augmented-wave method, Phys. Rev. B 59 (1999) 1758, https://doi.org/10.1103/PhysRevB.59.1758.

[28] J.P. Perdew, K. Burke, M. Ernzerhof, Generalized gradient approximation made simple, Phys. Rev. Lett. 77 (1996) 3865, https://doi.org/10.1103/PhysRevLett.77.3865.

[29] H.J. Monkhorst, J.D. Pack, Special points for Brillouin-zone integrations, Phys. Rev. B 13 (1976) 5188, https://doi.org/10.1103/PhysRevB.13.5188.

[30] L. Chaput, Direct solution to the linearized phonon Boltzmann equation, Phys. Rev. Lett. 110 (2013) 265506, https://doi.org/10.1103/PhysRevLett.110.265506.

[31] A. Togo, L. Chaput, T. Tadano, I. Tanaka, Implementation strategies in phonopy and phono3py, J. Phys. Condens. Matter 35 (2023) 353001, https://doi.org/10.1088/1361-648X/acd831.

[32] A. Togo, I. Tanaka, First principles phonon calculations in materials science, Scr Mater 108 (2015) 1–5, https://doi.org/10.1016/j.scriptamat.2015.07.021.

[33] K. Parlinski, Z.Q. Li, Y. Kawazoe, First-principles determination of the soft mode in cubic ZrO2, Phys. Rev. Lett. 78 (1997) 4063–4066, https://doi.org/10.1103/PhysRevLett.78.4063.

[34] P. Giannozzi, S. de Gironcoli, P. Pavone, S. Baroni, Ab initio calculation of phonon dispersions in semiconductors, Phys. Rev. B 43 (1991) 7231–7242, https://doi.org/10.1103/PhysRevB.43.7231.

[35] A. Van de Walle, M. Asta, G. Ceder, The alloy theoretic automated toolkit: a user guide, Calphad 26 (2002) 539–553, https://doi.org/10.1016/S0364-5916(02)80006-2.

[36] F. Körmann, Y. Ikeda, B. Grabowski, M.H.F. Sluiter, Phonon broadening in high entropy alloys, npj Comput. Mater. 3 (1 3) (2017) 1–9, https://doi.org/10.1038/s41524-017-0037-8.

[37] S.R. Turner, S. Pailhès, F. Bourdarot, J. Ollivier, Y. Sidis, J.-P. Castellan, J.-M. Zanotti, Q. Berrod, F. Porcher, A. Bosak, M. Feuerbacher, H. Schober, M. de Boissieu, V.M. Giordano, Phonon behavior in a random solid solution: a lattice dynamics study on the high-entropy alloy FeCoCrMnNi, Nat. Commun. 13 (2022) 7509, https://doi.org/10.1038/s41467-022-35125-4.

[38] X. Gu, Y. Wei, X. Yin, B. Li, R. Yang, Colloquium: phononic thermal properties of two-dimensional materials, Rev. Mod. Phys. 90 (2018) 041002, https://doi.org/10.1103/RevModPhys.90.041002.

[39] A. Cepellotti, G. Fugallo, L. Paulatto, M. Lazzeri, F. Mauri, N. Marzari, Phonon hydrodynamics in two-dimensional materials, Nat. Commun. 6 (2015) 6400, https://doi.org/10.1038/ncomms7400.

[40] G. Qin, Z. Qin, W.-Z. Fang, L.-C. Zhang, S.-Y. Yue, Q.-B. Yan, M. Hu, G. Su, Diverse anisotropy of phonon transport in two-dimensional group IV–VI compounds: a comparative study, Nanoscale 8 (2016) 11306–11319, https://doi.org/10.1039/C6NR01349J.

[41] X. Gu, R. Yang, Phonon transport in single-layer transition metal dichalcogenides: a first-principles study, Appl. Phys. Lett. 105 (2014) 131903, https://doi.org/10.1063/1.4896685.

[42] S. Karak, J. Bera, S. Paul, S. Sahu, S. Saha, Low thermal conductivity and interface thermal conductance in SnS_2, Phys. Rev. B 104 (2021) 195304, https://doi.org/10.1103/PhysRevB.104.195304.

[43] G. Liu, Z. Gao, G.-L. Li, H. Wang, Abnormally low thermal conductivity of 2D selenene: an ab initio study, J. Appl. Phys. 127 (2020) 065103, https://doi.org/10.1063/1.5135092.
[44] Z. Gao, F. Tao, J. Ren, Unusually low thermal conductivity of atomically thin 2D tellurium, Nanoscale 10 (2018) 12997–13003, https://doi.org/10.1039/C8NR01649F.
[45] W. Zhai, L. Li, M. Zhao, Q. Hu, J. Li, G. Yang, Y. Yan, C. Zhang, P.-F. Liu, A novel 2D material with intrinsically low thermal conductivity of Ga_2O_3 (100): first-principles investigations, Phys. Chem. Chem. Phys. 24 (2022) 4613–4619, https://doi.org/10.1039/D1CP05413A.
[46] R. Attri, S. Roychowdhury, K. Biswas, C.N.R. Rao, Low thermal conductivity of 2D borocarbonitride nanosheets, J. Solid State Chem. 282 (2020) 121105, https://doi.org/10.1016/j.jssc.2019.121105.
[47] M.W. Barsoum, I. Salama, T. El-Raghy, J. Golczewski, H.J. Seifert, F. Aldinger, W. D. Porter, H. Wang, Thermal and electrical properties of Nb_2AlC, $(Ti, Nb)_2AlC$ and Ti_2AlC, Metall. Mater. Trans. 33 (2002) 2775–2779, https://doi.org/10.1007/s11661-002-0262-7.
[48] J.D. Hettinger, S.E. Lofland, P. Finkel, T. Meehan, J. Palma, K. Harrell, S. Gupta, A. Ganguly, T. El-Raghy, M.W. Barsoum, Electrical transport, thermal transport, and elastic properties of M_2AlC (M=Ti, Cr, Nb, and V), Phys. Rev. B 72 (2005) 115120, https://doi.org/10.1103/PhysRevB.72.115120.
[49] G.A. Slack, Nonmetallic crystals with high thermal conductivity, J. Phys. Chem. Solid. 34 (1973) 321–335, https://doi.org/10.1016/0022-3697(73)90092-9.
[50] R.F. Wallis, Surface effects on lattice vibrations, Surf. Sci. 2 (1964) 146–155, https://doi.org/10.1016/0039-6028(64)90053-6.
[51] G.P. Srivastava, The Physics of Phonons, CRC Press, Boca Raton, 2022, https://doi.org/10.1201/9781003141273.
[52] G.P. Srivastava, Phonon conductivity of insulators and semiconductors, J. Phys. Chem. Solid. 41 (1980) 357–368, https://doi.org/10.1016/0022-3697(80)90210-3.
[53] K. Kim, J. He, B. Ganeshan, J. Liu, Disorder enhanced thermal conductivity anisotropy in two-dimensional materials and van der Waals heterostructures, J. Appl. Phys. 124 (2018) 055104, https://doi.org/10.1063/1.5031147.
[54] E. Osei-Agyemang, G. Balasubramanian, Understanding the anisotropic phonon thermal transport through 2D β-siligraphene, Carbon N Y 179 (2021) 523–530, https://doi.org/10.1016/j.carbon.2021.04.071.
[55] J. He, Y. Xia, S.S. Naghavi, V. Ozoliņš, C. Wolverton, Designing chemical analogs to PbTe with intrinsic high band degeneracy and low lattice thermal conductivity, Nat. Commun. 10 (2019) 719, https://doi.org/10.1038/s41467-019-08542-1.
[56] X. Shi, X. Zhang, A. Ganose, J. Park, C. Sun, Z. Chen, S. Lin, W. Li, A. Jain, Y. Pei, Compromise between band structure and phonon scattering in efficient n-Mg_3Sb_2-Bi thermoelectrics, Mater. Today Phys. 18 (2021) 100362, https://doi.org/10.1016/j.mtphys.2021.100362.
[57] S.-F. Wang, Z.-G. Zhang, B.-T. Wang, J.-R. Zhang, F.-W. Wang, Intrinsic ultralow lattice thermal conductivity in the full-heusler compound Ba_2AgSb, Phys. Rev. Appl. 17 (2022) 034023, https://doi.org/10.1103/PhysRevApplied.17.034023.
[58] X. Song, Y. Zhao, J. Ni, S. Meng, Z. Dai, Strong anharmonic phonon scattering and superior thermoelectric properties of Li_2NaBi, Mater. Today Phys. 31 (2023) 100990, https://doi.org/10.1016/j.mtphys.2023.100990.
[59] M.T. Dove, Anharmonic effects and phase transitions, in: Introduction to Lattice Dynamics, Cambridge University Press, 1993, pp. 101–131, https://doi.org/10.1017/CBO9780511619885.010.
[60] J.M. Ziman, Phonon-phonon interaction, in: Electrons and Phonons, Oxford University Press, 2001, pp. 128–158, https://doi.org/10.1093/acprof:oso/9780198507796.003.0003.
[61] C. Herring, Role of low-energy phonons in thermal conduction, Phys. Rev. 95 (1954) 954–965, https://doi.org/10.1103/PhysRev.95.954.
[62] P.C.K. Kwok, Green's Function Method in Lattice Dynamics, Solid State Phys. 20 (1968) 213–303, https://doi.org/10.1016/S0081-1947(08)60219-2.
[63] P. Singh, C. Acemi, A. Kuchibhotla, B. Vela, P. Sharma, W. Zhang, P. Mason, G. Balasubramanian, I. Karaman, R. Arroyave, M.C. Hipwell, D.D. Johnson, Alloying Effects on the Transport Properties of Refractory High-Entropy Alloys, 2024, https://doi.org/10.2139/ssrn.4723754.
[64] Z. Zhao, H. Xiang, H. Chen, F.Z. Dai, X. Wang, Z. Peng, Y. Zhou, High-entropy $(Nd_{0.2}Sm_{0.2}Eu_{0.2}Y_{0.2}Yb_{0.2})_4Al_2O_9$ with good high temperature stability, low thermal conductivity, and anisotropic thermal expansivity, J. Adv. Ceram. 9 (5) (2020) 595–605, https://doi.org/10.1007/S40145-020-0399-0.